

Solving nonconvex Hamilton–Jacobi–Isaacs equations with PINN-based policy iteration

Hee Jun Yang^{*} Minjung Gim^{*} Yeoneung Kim[†]

July 22, 2025

Abstract

We propose a mesh-free policy iteration framework that combines classical dynamic programming with physics-informed neural networks (PINNs) to solve high-dimensional, nonconvex Hamilton–Jacobi–Isaacs (HJI) equations arising in stochastic differential games and robust control. The method alternates between solving linear second-order PDEs under fixed feedback policies and updating the controls via pointwise minimax optimization using automatic differentiation. Under standard Lipschitz and uniform ellipticity assumptions, we prove that the value function iterates converge locally uniformly to the unique viscosity solution of the HJI equation. The analysis establishes equi-Lipschitz regularity of the iterates, enabling provable stability and convergence without requiring convexity of the Hamiltonian. Numerical experiments demonstrate the accuracy and scalability of the method. In a two-dimensional stochastic path-planning game with a moving obstacle, our method matches finite-difference benchmarks with relative L^2 -errors below 10^{-2} . In five- and ten-dimensional publisher–subscriber differential games with anisotropic noise, the proposed approach consistently outperforms direct PINN solvers, yielding smoother value functions and lower residuals. Our results suggest that integrating PINNs with policy iteration is a practical and theoretically grounded method for solving high-dimensional, nonconvex HJI equations, with potential applications in robotics, finance, and multi-agent reinforcement learning.

1 Introduction

The Hamilton–Jacobi–Isaacs (HJI) equation plays a fundamental role in differential games and robust control, characterizing the value function of zero-sum stochastic dynamic games. In the presence of diffusion, the HJI equation takes the form

$$\partial_t v + H(t, x, \nabla_x v) = -\frac{1}{2} \text{Tr}(\sigma \sigma^\top D_{xx}^2 v),$$

with suitable terminal condition. The Hamiltonian H typically involves a minimax operation over control variables and may be nonconvex or nonsmooth, which presents substantial analytical and numerical challenges.

Classical numerical methods, such as finite difference and semi-Lagrangian schemes [2, 16, 22], provide robust convergence guarantees via viscosity solution theory, but their reliance on structured spatial meshes renders them intractable in high dimensions due to the curse of dimensionality. Various extensions using unstructured meshes [3], convexification [15], and radial basis collocation [4, 7] have been proposed, but scalability remains a limiting factor.

To alleviate grid-related bottlenecks, mesh-free methods based on physics-informed neural networks (PINNs) [10, 20] have emerged as promising alternatives. PINNs approximate solutions of PDEs by minimizing residuals through neural networks with automatic differentiation, and have been applied to Hamilton–Jacobi (HJ) and Hamilton–Jacobi–Bellman (HJB) equations. Recent studies [19] demonstrate improved convergence in nonconvex HJ settings using adaptive losses. However, directly minimizing nonconvex residuals can be unstable and prone to poor local minima, especially when the Hamiltonian involves a nonsmooth minimax structure.

^{*}National Institute for Mathematical Sciences, Daejeon 34047, Republic of Korea. E-mail: yangheejun1009@nims.re.kr, mjgim@nims.re.kr.

[†]Corresponding author. Department of Applied Artificial Intelligence, SeoulTech, E-mail: yeoneung@seoultech.ac.kr.

To address these limitations, policy iteration (PI) methods have been introduced for HJB/HJI equations [9, 12, 13, 24]. By alternating between value evaluation and policy improvement steps, PI offers a structured approach that improves stability and convergence. When coupled with PINNs, this framework enables mesh-free iteration and can mitigate difficulties associated with nonconvexity in the Hamiltonian. In particular, Lee and Kim [18] proposed a PI framework based on deep operator learning (DeepONet) to solve Hamilton–Jacobi–Bellman equations, proposing the first operator-learning-based implementation of policy iteration for HJB equations. Their approach emphasized function-space policy updates via neural operators and showed promising results in high-dimensional optimal control problems. Our method departs from this line by adopting a residual-based PINN formulation tailored to nonconvex HJI equations, while providing a rigorous convergence guarantee under ellipticity assumptions.

In this paper, we propose a PINN-based policy iteration framework for solving nonconvex HJI equations. At each step, the value function is approximated by a neural network trained to minimize the PDE residual for fixed policies. Gradients from automatic differentiation are used to update feedback controls via pointwise optimization. This leads to a continuous optimization framework that avoids spatial grids entirely. We establish convergence to the viscosity solution under standard Lipschitz assumptions. In addition to empirical performance, the proposed method offers a structural advantage: it allows for explicit control over approximation errors via provable L^2 bounds, something rarely feasible in nonconvex HJI problems.

The rest of the paper is organized as follows. In Section 2, we briefly review the formulation of Hamilton–Jacobi–Isaacs equations in the context of differential games. Section 3 presents the proposed PINN-based policy iteration framework, detailing the policy evaluation and improvement steps, the associated training procedure, and a theoretical analysis of the method, including a convergence guarantee under suitable regularity and ellipticity conditions. Section 4 presents the results of extensive numerical experiments on benchmark problems in multiple dimensions, highlighting the accuracy, scalability, and robustness of the proposed approach. Finally, Section 5 concludes the paper and discusses potential directions for future research.

2 Stochastic Differential Games and Hamilton–Jacobi–Isaacs equations

Given $0 \leq t < T$, $d, m_1, m_2 \in \mathbb{N}$, $A \subset \mathbb{R}^{m_1}$ and $B \subset \mathbb{R}^{m_2}$, we consider a two-player zero-sum stochastic differential game over a finite horizon $[0, T]$, where the state process $X(s) \in \mathbb{R}^d$ evolves according to the controlled stochastic differential equation

$$\begin{cases} dX(s) &= f(X(s), a(s), b(s))ds + \sigma(s, X(s))dW_s, \quad \text{for } s \geq t, \\ X(t) &= x, \end{cases} \quad (2.1)$$

where $W_s \in \mathbb{R}^d$ denotes a standard d -dimensional Brownian motion and the functions $f : \mathbb{R}^d \times A \times B \rightarrow \mathbb{R}^d$ and $\sigma : [0, T] \times \mathbb{R}^d \rightarrow \mathbb{R}^{d \times d}$ represent the drift and diffusion coefficients, respectively. Let $\mathcal{F} := (\mathcal{F}_s)_{s \geq 0}$ be the filtration generated by $(W_s)_{s \geq 0}$, and for $s \in [t, T]$, set $a \in \mathcal{A}_t$ and $b \in \mathcal{B}_t$ where

$$\begin{cases} \mathcal{A}_t &= \{a : [t, T] \rightarrow A \mid a \text{ is a } \{\mathcal{F}_s\}_{s \in [t, T]} \text{-adapted process}\}, \\ \mathcal{B}_t &= \{b : [t, T] \rightarrow B \mid b \text{ is a } \{\mathcal{F}_s\}_{s \in [t, T]} \text{-adapted process}\}. \end{cases}$$

The performance of a control pair $(a, b) \in \mathcal{A}_t \times \mathcal{B}_t$ is evaluated through the cost functional

$$J(t, x; a, b) = \mathbb{E}\left[\int_t^T c(X(s), a(s), b(s))ds + g(X_T)\right],$$

where $c : \mathbb{R}^d \times A \times B \rightarrow \mathbb{R}$ is the running cost, and $g : \mathbb{R}^d \rightarrow \mathbb{R}$ is the terminal cost. Player I seeks to minimize this expected cost, while Player II aims to maximize it. The set of admissible nonanticipative strategies for Player II beginning at time t is defined by

$$\Gamma_t = \{\beta : \mathcal{A}_t \rightarrow \mathcal{B}_t \mid \text{nonanticipating}\},$$

where the strategy β is called nonanticipative if, for $a_1, a_2 \in \mathcal{A}_t$ and $s \in [t, T]$,

$$a_1(\cdot) = a_2(\cdot) \text{ on } [t, s] \implies \beta[a_1](\cdot) = \beta[a_2](\cdot) \text{ on } [t, s].$$

Accordingly, the value function of the game is defined as

$$v(t, x) = \sup_{\beta \in \Gamma_t} \inf_{a \in \mathcal{A}_t} J(t, x; a, \beta[a]).$$

Under standard regularity assumptions, such as Lipschitz continuity and boundedness of f , c , and σ in both x and t , and uniform ellipticity of the matrix $\sigma(t, x)\sigma^\top(t, x)$, the value function $v(t, x)$ satisfies the dynamic programming principle and is characterized as the unique viscosity solution of the Hamilton–Jacobi–Isaacs (HJI) equation

$$\begin{cases} \partial_t v(t, x) + H(t, x, \nabla_x v(t, x)) = -\frac{1}{2} \text{Tr}(\sigma \sigma^\top(t, x) D_{xx}^2 v(t, x)), & \text{in } (0, T) \times \mathbb{R}^d, \\ v(T, x) = g(x) & \text{on } \mathbb{R}^d, \end{cases}$$

where $H(t, x, p) := \sup_{\mathbf{b} \in B} \inf_{\mathbf{a} \in A} L(t, x, p)(\mathbf{a}, \mathbf{b})$ with $L(t, x, p)(\mathbf{a}, \mathbf{b}) := c(t, x, \mathbf{a}, \mathbf{b}) + p \cdot f(t, x, \mathbf{a}, \mathbf{b})$.

3 Physics-informed approach for solving HJI equations

3.1 Policy iteration for HJI equations

We begin by introducing the notation used throughout the paper. For $x \in \mathbb{R}^d$, we write $|x|$ for the Euclidean norm. Given a function $f : \Omega \rightarrow \mathbb{R}^n$, we denote its standard L^p norm by

$$\|f\|_p := \left(\int_{\Omega} |f|^p dx \right)^{1/p}, \quad \text{for } p \in (0, \infty],$$

where $|f|$ denotes the pointwise Euclidean norm of f . We denote by $\text{Lip}(\Omega)$ the set of Lipschitz continuous functions on Ω , and by $C(\Omega)$ the set of continuous functions.

We now introduce the policy iteration framework used throughout the paper. Our goal is to solve high-dimensional Hamilton–Jacobi–Isaacs (HJI) equations by combining policy iteration with physics-informed neural networks (PINNs). The proposed method alternates between solving linear PDEs under fixed feedback policies and updating the feedback controls via gradient-based minimax steps.

As a starting point, we follow the iterative scheme introduced in [9], where a discrete-time policy iteration (PI) algorithm for the HJI equation is first proposed based on the mesh-free algorithm, which is demonstrated in Algorithm 1.

Algorithm 1 Mesh-free Policy Iteration for HJI

Input: Lipschitz continuous initial feedback (α_0, β_0)

1: **for** $n = 0, 1, 2, \dots$ **do**

2: **Policy evaluation:** find v_n solving

$$\partial_t v_n + L(t, x, \nabla_x v_n)(\alpha_n, \beta_n) = -\frac{1}{2} \text{Tr}(\sigma \sigma^\top D_{xx}^2 v_n), \quad v_n(T, x) = g(x).$$

3: **Policy improvement:** at each (t, x) with gradient $p = \nabla_x v_n(t, x)$,

$$\alpha_{n+1,b}(t, x) \leftarrow \arg \min_{\mathbf{a} \in A} L(t, x, p)(\mathbf{a}, b),$$

$$\beta_{n+1}(t, x) \leftarrow \arg \max_{\mathbf{b} \in B} L(t, x, p)(\alpha_{n+1,b}(t, x), \mathbf{b}),$$

$$\alpha_{n+1}(t, x) \leftarrow \alpha_{n+1,\beta_{n+1}(t,x)}(t, x).$$

4: **end for**

Output: converged feedback pair (α_n, β_n) and value v_n

In their setting, the diffusion matrix σ may be degenerate, and the value function v can fail to be differentiable, making the feedback-based policy update

$$(a, b) \mapsto \arg \min_{a \in A} \arg \max_{b \in B} L(t, x, \nabla_x v)(a, b)$$

ill-posed. To address this, the authors of [9] introduced a discrete space-time grid and an artificial viscosity term that ensures enough regularity to define the minimax update at grid points. Convergence to the viscosity solution is then obtained via a careful limiting argument.

In contrast, we assume that the coefficients f , c , and σ are Hölder continuous in (t, x) and that the terminal cost $g \in C^{2+\beta}(\mathbb{R}^d)$, we obtain, via Schauder theory, that each value function v_n belongs to $C^{2+\beta}$ in space variable x , and hence, has Lipschitz continuous gradients $\nabla_x v_n$ with respect to x .

As a result, the updated feedback policies $(\alpha_{n+1}, \beta_{n+1})$, defined through pointwise minimization and maximization over continuous maps composed with $\nabla_x v_n$, are themselves Lipschitz continuous. This eliminates the need for measurable selection arguments entirely and guarantees well-posedness of the policy update step. Moreover, this smoothness facilitates stable PINN optimization and improves generalization across iterations.

We recall the form of the Lagrangian

$$L(t, x, p)(\mathbf{a}, \mathbf{b}) := c(t, x, \mathbf{a}, \mathbf{b}) + p \cdot f(t, x, \mathbf{a}, \mathbf{b}),$$

and introduce assumptions on the dynamics and cost function.

Assumption 1. *We impose the following assumptions throughout the paper.*

- The control sets $A \subset \mathbb{R}^{m_1}$ and $B \subset \mathbb{R}^{m_2}$ are convex and compact. For each fixed $(t, x, p) \in [0, T] \times \mathbb{R}^d \times \mathbb{R}^d$, the map

$$(\mathbf{a}, \mathbf{b}) \mapsto L(t, x, p)(\mathbf{a}, \mathbf{b}) := c(t, x, \mathbf{a}, \mathbf{b}) + p \cdot f(t, x, \mathbf{a}, \mathbf{b})$$

is μ_A -strongly convex in \mathbf{a} and μ_B -strongly concave in \mathbf{b} .

That is, for every (t, x, p) , the maps

$$\mathbf{a} \mapsto L(t, x, p)(\mathbf{a}, \mathbf{b}) \quad \text{and} \quad \mathbf{b} \mapsto L(t, x, p)(\mathbf{a}, \mathbf{b})$$

are strongly convex and strongly concave, respectively, uniformly in (t, x, p) .

- The functions f , c , g , and σ are bounded and Lipschitz continuous in all variables, with common Lipschitz constant $L_u > 0$. In addition, there exists $\beta > 0$ such that:

- The terminal cost satisfies $g \in C^{2+\beta}(\mathbb{R}^d) \cap L^2(\mathbb{R}^d)$;
- The running cost satisfies

$$\sup_{(a, b) \in A \times B} \|c(\cdot, \cdot, a, b)\|_{L^\infty(0, T; L^2(\mathbb{R}^d))} < \infty;$$

- The mappings $(t, x) \mapsto f(t, x, \mathbf{a}, \mathbf{b})$ and $\sigma(t, x)$ belong to $C^\beta([0, T] \times \mathbb{R}^d)$, uniformly in (\mathbf{a}, \mathbf{b}) .

- The diffusion coefficient $\sigma \in C([0, T] \times \mathbb{R}^d; \mathbb{R}^{d \times d})$ is uniformly elliptic: there exists $\lambda > 0$ such that

$$\sigma(t, x)\sigma(t, x)^\top \succeq \lambda I_d \quad \text{for all } (t, x) \in [0, T] \times \mathbb{R}^d.$$

The assumptions stated above lead to a mild structural property of the policy-update map; this property, formulated below, is central to our convergence analysis.

Lemma 1 (Lipschitz continuity of the feedback selector). *Let the Lagrangian $L(t, x, p)(\mathbf{a}, \mathbf{b}) := c(t, x, \mathbf{a}, \mathbf{b}) + p \cdot f(t, x, \mathbf{a}, \mathbf{b})$. Then for every (t, x, p) , the policy update*

$$\begin{cases} \alpha^*(t, x, p) &= \operatorname{argmin}_{\mathbf{a} \in A} L(t, x, p)(\mathbf{a}, \beta^*(t, x, p)), \\ \beta^*(t, x, p) &= \operatorname{argmax}_{\mathbf{b} \in B} L(t, x, p)(\alpha^*(t, x, p), \mathbf{b}), \end{cases}$$

admits a unique solution, and (α^*, β^*) is globally Lipschitz in p :

$$|\alpha^*(t, x, p_1) - \alpha^*(t, x, p_2)| + |\beta^*(t, x, p_1) - \beta^*(t, x, p_2)| \leq \kappa |p_1 - p_2|,$$

with a constant $\kappa > 0$.

Proof. For $p \in \mathbb{R}^d$, set $F_p := (\nabla_{\mathbf{a}} L_p, -\nabla_{\mathbf{b}} L_p)$. Since L_p is μ_A -strongly convex in \mathbf{a} and μ_B -strongly concave in \mathbf{b} , F_p is μ -strongly monotone with $\mu := \min\{\mu_A, \mu_B\}$:

$$\langle F_p(z_1) - F_p(z_2), z_1 - z_2 \rangle \geq \mu |z_1 - z_2|^2, \quad \text{for } z_i = (\mathbf{a}_i, \mathbf{b}_i) \in A \times B.$$

For every momentum p the saddle point $z^*(p) := (\alpha^*(t, x, p), \beta^*(t, x, p))$ is the unique solution of the variational inequality

$$\langle F_p(z^*(p)), z - z^*(p) \rangle \geq 0 \quad \text{for } z \in A \times B.$$

Let $p_1, p_2 \in \mathbb{R}^d$ and abbreviate $z_i := z^*(p_i)$. Choosing $z = z_2$ for p_1 and $z = z_1$ in the for p_2 gives

$$\langle F_{p_1}(z_1), z_2 - z_1 \rangle \geq 0 \quad \text{and} \quad \langle F_{p_2}(z_2), z_1 - z_2 \rangle \geq 0.$$

Adding these inequalities yields

$$\langle F_{p_1}(z_1) - F_{p_2}(z_2), z_1 - z_2 \rangle \leq 0,$$

and therefore, we have

$$\begin{aligned} \mu |z_1 - z_2|^2 &\leq \langle F_{p_1}(z_1) - F_{p_1}(z_2), z_1 - z_2 \rangle \\ &= \langle F_{p_1}(z_1) - F_{p_2}(z_2), z_1 - z_2 \rangle + \langle F_{p_2}(z_2) - F_{p_1}(z_2), z_1 - z_2 \rangle \\ &\leq |F_{p_2}(z_2) - F_{p_1}(z_2)| |z_1 - z_2|. \end{aligned}$$

Because L is globally Lipschitz in the p , we have

$$|F_{p_2}(z_2) - F_{p_1}(z_2)| \leq C |p_1 - p_2|.$$

Combining the inequalities yields the desired estimate. \square

The next result is a direct analogue of [9][Theorem 1.1] but specialized to the uniformly elliptic case and stated in continuous time.

Theorem 1 (Convergence of policy iteration under uniform ellipticity). *Suppose Assumption 1 holds and let $T > 0$ be given. Let $\{v_n\}_{n \geq 0}$ be the sequence of value functions following Algorithm 1 with $L(t, x, p)(\mathbf{a}, \mathbf{b}) := c(t, x, \mathbf{a}, \mathbf{b}) + p \cdot f(t, x, \mathbf{a}, \mathbf{b})$. Then, the sequence $\{v_n\}$ converges locally uniformly to a function v , which is the unique bounded, continuous viscosity solution of the HJI equation:*

$$\begin{cases} \partial_t v + H(t, x, \nabla_x v) = -\frac{1}{2} \text{Tr}(\sigma \sigma^\top(t, x) D_{xx}^2 v) & \text{in } [0, T] \times \mathbb{R}^d, \\ v(T, x) = g(x), & \text{on } \mathbb{R}^d. \end{cases} \quad (3.1)$$

Proof. For each $n \geq 0$ let v_n be the bounded and continuous viscosity solution [5] of the policy evaluation problem

$$\begin{cases} \partial_t v_n + L(t, x, \nabla_x v_n)(\alpha_n, \beta_n) = -\frac{1}{2} \text{Tr}(\sigma \sigma^\top(t, x) D_{xx}^2 v_n), & \text{in } [0, T] \times \mathbb{R}^d, \\ v_n(T, x) = g(x), & \text{on } \mathbb{R}^d. \end{cases}$$

With $b_n(t, x) := f(t, x, \alpha_n, \beta_n)$ and $c_n(t, x) := c(t, x, \alpha_n, \beta_n)$, we recall the standard Feynman–Kac representation [8]:

$$v_n(t, x) = \mathbb{E}[g(X_T^{t,x}) + \int_t^T c_n(s, X_s^{t,x}) ds],$$

where $X_s^{t,x}$ solves $dX_s^{t,x} = b_n(s, X_s^{t,x}) ds + \sigma(s, X_s^{t,x}) dW_s$ with $X_t^{t,x} = x$. Since g and c_n are bounded, we have

$$|v_n(t, x)| \leq \mathbb{E}[|g(X_T^{t,x})|] + \mathbb{E}\left[\int_t^T |c_n(s, X_s^{t,x})| ds\right] \leq \|g\|_\infty + T \|c_n\|_\infty.$$

Therefore, we have the uniform bound of v_n independent of n , which is given by

$$\|v_n\|_{L^\infty} \leq \|g\|_\infty + T\|c_n\|_\infty =: M.$$

Fix any $x, y \in \mathbb{R}^d$ and $t \in [0, T]$. For a given index n consider the coupled SDEs

$$\begin{aligned} dX_s^{t,x} &= b_n(s, X_s^{t,x})ds + \sigma(s, X_s^{t,x})dW_s, & X_t^{t,x} &= x, \\ dX_s^{t,y} &= b_n(s, X_s^{t,y})ds + \sigma(s, X_s^{t,y})dW_s, & X_t^{t,y} &= y, \end{aligned}$$

where both processes are driven by the same Brownian motion W_s . Denoting $\Delta_s := X_s^{t,x} - X_s^{t,y}$, we deduce that $\frac{d}{ds}\mathbb{E}[|\Delta_s|^2] \leq C\mathbb{E}[|\Delta_s|^2]$ by the Lipschitz continuity of b_n and σ . Hence, by the Gronwall inequality,

$$\mathbb{E}[|\Delta_s|^2] \leq e^{C(s-t)}|x - y|^2,$$

which implies that

$$\mathbb{E}[|\Delta_s|] \leq e^{C(s-t)}|x - y|, \quad t \leq s \leq T.$$

Therefore, we have that

$$v_n(t, z) = \mathbb{E}[g(X_T^{t,z}) + \int_t^T c_n(s, X_s^{t,z})ds], \quad z \in \{x, y\}.$$

Subtracting the two instances and applying the Lipschitz bounds, we have

$$\begin{aligned} |v_n(t, x) - v_n(t, y)| &\leq \mathbb{E}[|g(X_T^{t,x}) - g(X_T^{t,y})|] + \mathbb{E}\left[\int_t^T |c_n(s, X_s^{t,x}) - c_n(s, X_s^{t,y})|ds\right] \\ &\leq C(\mathbb{E}[|\Delta_T|] + \int_t^T \mathbb{E}[|\Delta_s|]ds) \\ &\leq C|x - y|(e^{L(T-t)} + \int_t^T e^{L(s-t)}ds) \\ &\leq C_T|x - y|, \end{aligned}$$

which ensures the uniform Lipschitz continuity of $v'_n s$ in x .

Next, we fix $x \in \mathbb{R}^d$ and $0 < h \leq T - t$. By the dynamic programming principle,

$$v_n(t, x) = \mathbb{E}[v_n(t+h, X_{t+h}^{t,x}) + \int_t^{t+h} c_n(s, X_s^{t,x})ds].$$

Subtracting $v_n(t+h, x)$, we have

$$|v_n(t+h, x) - v_n(t, x)| \leq \mathbb{E}[|v_n(t+h, x) - v_n(t+h, X_{t+h}^{t,x})|] + \|c_n\|_\infty h.$$

From the spatial Lipschitz continuity of v_n and the estimate

$$\mathbb{E}[|X_{t+h}^{t,x} - x|] \leq C\sqrt{h},$$

where C depends only on $\|c\|_\infty$ and $\|\sigma\|_\infty$, we obtain

$$|v_n(t+h, x) - v_n(t, x)| \leq C\sqrt{h},$$

where C depends only on the uniform bounds $\|c\|_\infty$, $\|\sigma\|_\infty$ and $\|f\|_\infty$ (by Assumption 1) and hence is independent of n . We thus obtain

$$|v_n(t+h, x) - v_n(t, x)| \leq C\sqrt{h},$$

Invoking Lemma 1, the feedback pair $(\alpha_{n+1}, \beta_{n+1})$ is Lipschitz continuous and well-defined. Additionally, by the Arzela–Ascoli theorem, for each sequence $\{v_n\}$, there exists a subsequence converging uniformly to v that is Lipschitz continuous. Finally, by the stability property of the viscosity solution [25], v solves (3.1) in the viscosity sense. \square

To rigorously quantify the convergence behavior of the proposed scheme, we establish an exponential rate under the assumptions introduced earlier. Crucially, the analysis relies on the equi-Lipschitz property of the value function iterates, which not only guarantees compactness and stability but also enables a well-defined feedback update at each step.

The proof of Proposition 1 builds upon prior analyses of localized L^2 energy estimates for policy iteration, developed in [23, 24]. These works focused on bounding the propagation of approximation errors in the L^2 norm through energy estimates and Gronwall-type arguments. In contrast, the recent work of Guo, Tang, and Zhang [9] introduced a novel analytical approach to establish pointwise (L^∞) convergence rates using a different argument structure based on a novel temporal-spatial discretization. Our analysis adheres to the L^2 route, which is particularly applicable to rigorous control of residuals in the PINN-based implementation, and yields an explicit exponential rate.

Proposition 1 (Uniform exponential convergence rate). *Fix $T > 0$ and assume that Assumption 1 is satisfied. Let $\{v_n\}_{n \geq 0}$ be the sequence generated by the policy iteration algorithm described in Theorem 1. We denote by v the unique bounded viscosity solution to the Hamilton–Jacobi–Isaacs equation (3.1). Then there exists $\rho \in (0, 1)$ and a constant C such that for every $n \geq 0$*

$$\sup_{t \in [0, T]} \|v_n(t, \cdot) - v(t, \cdot)\|_2 \leq C\rho^n.$$

Proof. Throughout the proof we write

$$\delta_n := v_{n+1} - v_n, \quad e_n := v - v_n, \quad \pi_n := (\alpha_n, \beta_n).$$

Reversing the time, we may consider $[0, T] \times \mathbb{R}^d$ with $e_n(0, x) = \delta_n(0, x) = 0$ for all $n \geq 0$. Let us define

$$\mathcal{L}_n := L(t, x, \nabla_x v_{n+1})(\pi_{n+1}) - L(t, x, \nabla_x v_n)(\pi_n).$$

Since

$$\mathcal{L}_n = \underbrace{L(t, x, \nabla_x v_{n+1})(\pi_{n+1}) - L(t, x, \nabla_x v_n)(\pi_{n+1})}_{=: \text{II}} - L(t, x, \nabla_x v_n)(\pi_n).$$

Clearly, $|\text{I}| \leq L_u |\nabla \delta_n|$. To bound II, let us recall the optimality condition of the Hamiltonian, which is

$$H(t, x, p_n) = L(t, x, p_n)(\pi_{n+1}), \quad \text{and} \quad H(t, x, p_{n-1}) = L(t, x, p_{n-1})(\pi_n),$$

where $p_n := \nabla_x v_n(t, x)$. Therefore,

$$\begin{aligned} |\text{II}| &= |H(t, x, p_n) - H(t, x, p_{n-1}) + H(t, x, p_{n-1}) - L(t, x, p_n)(\pi_n)| \\ &\leq |H(t, x, p_n) - H(t, x, p_{n-1})| + |L(t, x, p_{n-1})(\pi_n) - L(t, x, p_n)(\pi_n)| \\ &\leq 2L_u |p_n - p_{n-1}|, \end{aligned}$$

and we have that

$$|\mathcal{L}_n| \leq 2L_u (|\nabla_x \delta_n| + |\nabla_x \delta_{n-1}|). \quad (3.2)$$

Subtracting the two policy evaluation equations for v_{n+1} and v_n , multiplying by δ_n and integrating in space gives

$$\frac{d}{dt} \|\delta_n(t, \cdot)\|_2^2 + \lambda \|\nabla_x \delta_n(t, \cdot)\|_2^2 = -2 \int_{\mathbb{R}^d} \mathcal{L}_n \delta_n dx. \quad (3.3)$$

We first deduce that

$$2 \int_{\mathbb{R}^d} |\mathcal{L}_n \delta_n| dx \leq 4L_u (\|\nabla_x \delta_n(t, \cdot)\|_2 \|\delta_n(t, \cdot)\|_2 + \|\nabla_x \delta_{n-1}(t, \cdot)\|_2 \|\delta_n(t, \cdot)\|_2).$$

Invoking Young's inequality $ab \leq \frac{\eta}{2} a^2 + \frac{1}{2\eta} b^2$ with $\eta = \lambda/(4L_u)$ gives

$$2 \int_{\mathbb{R}^d} |\mathcal{L}_n \delta_n| dx \leq \frac{\lambda}{2} \|\nabla_x \delta_n(t, \cdot)\|_2^2 + \frac{\lambda}{2} \|\nabla_x \delta_{n-1}(t, \cdot)\|_2^2 + \frac{16L_u^2}{\lambda} \|\delta_n(t, \cdot)\|_2^2. \quad (3.4)$$

Combining (3.3)–(3.4) we obtain, for every $t \in [0, T]$,

$$\frac{d}{dt} \|\delta_n(t, \cdot)\|_2^2 + \frac{\lambda}{2} \|\nabla_x \delta_n(t, \cdot)\|_2^2 \leq \frac{16L_u^2}{\lambda} \|\delta_n(t, \cdot)\|_2^2 + \frac{\lambda}{2} \|\nabla_x \delta_{n-1}(t, \cdot)\|_2^2. \quad (3.5)$$

Define $E_n := \sup_{t \in [0, T]} \|\delta_n(t, \cdot)\|_2$ and $F_n := \sup_{t \in [0, T]} \|\nabla_x \delta_n(t, \cdot)\|_2$. Integrate (3.5) from 0 up to T and take the supremum in $t \in [0, T]$:

$$E_n^2 + \frac{\lambda}{2} \int_0^T \|\nabla_x \delta_n(t, \cdot)\|_2^2 dt \leq \frac{16L_u^2 T}{\lambda} E_n^2 + \frac{\lambda T}{2} F_{n-1}^2,$$

and hence,

$$E_n^2 \leq \frac{\lambda T}{2\mu} F_{n-1}^2, \quad (3.6)$$

where $\mu = 1 - \frac{16L_u^2 T}{\lambda}$. Since $\delta_n(0, x) = 0$, we invoke the gradient bound of δ_n demonstrated in [6], we have

$$\|\nabla_x \delta_n(t, \cdot)\|_2 \leq \tilde{C} \sqrt{T} (F_n + F_{n-1}).$$

We choose T small so that $\tilde{C} \sqrt{T} \leq \frac{1}{4}$, leading to

$$F_n \leq \rho F_{n-1} \quad \text{for} \quad \rho := \frac{\tilde{C} \sqrt{T}}{1 - \tilde{C} \sqrt{T}} \leq \frac{1}{3}. \quad (3.7)$$

Combining with (3.6), we get

$$\sup_{t \in [0, T]} \|v(t, \cdot) - v_n(t, \cdot)\|_2 \leq \sum_{k=n}^{\infty} E_k \leq C \rho^n.$$

Finally, we complete the proof as the same argument can be applied on subintervals

$$[0, T^*], [T^*, 2T^*], \dots, [(\ell - 1)T^*, \ell T^*],$$

for some $\ell \in \mathbb{N}$ satisfying $T/T^* \leq \ell$. □

Before proceeding to the theoretical convergence analysis in Theorem 1, we emphasize that our practical implementation employs a neural network representation for each value function iterate v_n . In particular, the PINN ansatz provides a globally defined function $v_n(t, x; \theta_n)$ whose gradients $\nabla_x v_n$ and Hessians $D_{xx}^2 v_n$ are computed via automatic differentiation and are therefore available almost everywhere. This regularity ensures that the policy improvement step, which requires pointwise minimization and maximization over control actions based on $\nabla_x v_n(t, x)$ is well-defined numerically across the training domain. Such an approach alleviates numerical difficulties observed in earlier studies of policy iteration, especially in settings where the value function is not smooth or only implicitly defined. Therefore, from a numerical perspective, the PINN-based policy iteration algorithm described above is fully implementable without ambiguity. This justifies our decision to first present the algorithmic formulation in full detail, before turning to the rigorous convergence analysis in the subsequent section.

3.2 PINN-Based Policy Iteration

For the fixed pair (α_n, β_n) the value function is represented by a neural network $v_n(t, x; \theta_n)$. Let $\{(t_j, x_j)\}_{j=1}^{N_{\text{int}}} \subset (0, T) \times \mathbb{R}^d$ be interior collocation points and $\{x_k^T\}_{k=1}^{N_{\text{bc}}} \subset \mathbb{R}^d$ terminal points. The network parameters are obtained by minimizing

$$\mathcal{J}(\theta_n) = \frac{1}{N_{\text{int}}} \sum_{j=1}^{N_{\text{int}}} |\partial_t v_n + L(t_j, x_j, \nabla_x v_n)(\alpha_n, \beta_n) + \frac{1}{2} \text{Tr}(a(t_j, x_j) D_{xx}^2 v_n)|^2 + \frac{1}{N_{\text{bc}}} \sum_{k=1}^{N_{\text{bc}}} |v_n(T, x_k^T) - g(x_k^T)|^2. \quad (3.8)$$

When implemented, we parameterize the value function $v_n(t, x; \theta_n)$ using the following ansatz:

$$v_n(t, x; \theta_n) = g(x) + (T - t)\mathcal{N}_n(t, x; \theta_n), \quad (3.9)$$

which explicitly enforces the terminal condition as a hard constraint, eliminating the need for a separate terminal loss term and thereby improving training stability and convergence speed [17].

All differential operators are evaluated by automatic differentiation. Because no spatial grid is required, the procedure scales to high state dimensions without suffering from the curse of dimensionality.

Algorithm 2 Mesh-free PINN Policy Iteration

Require: collocation sets $\{(t_j, x_j)\}$, terminal set $\{x_k^T\}$, tolerance tol , number of policy updates M , number of training epochs per policy update E

- 1: choose any Lipschitz continuous initial feedback pair $(\alpha_0, \beta_0) : [0, T] \times \mathbb{R}^d \rightarrow A \times B$
- 2: initialize network parameters θ_0 using Xavier initialization; set all biases to zero
- 3: **for** $n = 0, 1, 2, \dots, M - 1$ **do**
- 4: **for** $\ell = 1, \dots, E$ **do** ▷ Value evaluation
- 5: update θ_n of $v_n(t, x; \theta_n)$ via gradient descent to minimize $\mathcal{J}(\theta_n)$
- 6: **if** $\ell \equiv 0 \pmod{100}$ **then**
- 7: resample $\{(t_j, x_j)\}$ uniformly from $[0, T] \times \mathbb{R}^d$
- 8: **end if**
- 9: **end for**
- 10: **for all** collocation points (t, x) used in the gradient computation **do** ▷ Policy update
- 11: compute $\nabla_x v_n(t, x; \theta_n)$ via automatic differentiation
- 12: $\alpha_{n+1,b}(t, x) \leftarrow \arg \min_{\mathbf{a} \in A} L(t, x, \nabla_x v_n(t, x; \theta_n))(\mathbf{a}, b)$
- 13: $\beta_{n+1}(t, x) \leftarrow \arg \max_{\mathbf{b} \in B} L(t, x, \nabla_x v_n(t, x; \theta_n))(\alpha_{n+1,b}(t, x), \mathbf{b})$
- 14: $\alpha_{n+1}(t, x) \leftarrow \alpha_{n+1,\beta_{n+1}(t,x)}(t, x)$
- 15: **end for**
- 16: **if** $\|v_n - v_{n-1}\|_{L^\infty} < \text{tol}$ **then**
- 17: **break**
- 18: **end if**
- 19: next iteration by setting $\theta_{n+1} \leftarrow \theta_n$ ▷ Warm-start
- 20: **end for**

The implementation of the above policy iteration scheme relies on two key ingredients: (i) the ability to approximate value functions using neural networks trained on residual losses, and (ii) the ability to compute policy updates based on gradients obtained via automatic differentiation. Algorithm 2 outlines the resulting PINN-based scheme, where each policy update is executed in a completely mesh-free setting, leveraging the continuous feedback gradient $\nabla_x v_n(t, x)$.

Remark 1 (Comparison of Algorithm 1 and Algorithm 2). *Algorithm 1 describes an idealized policy iteration framework under which each value function v_n is assumed to solve a linear elliptic–parabolic PDE exactly, using classical analytic or grid-based numerical methods. This setting enables a rigorous convergence analysis under viscosity solution theory but is limited to low-dimensional problems due to the need for exact PDE solvers. In contrast, Algorithm 2 implements a practical mesh-free version based on physics-informed neural networks (PINNs). The value function v_n is approximated via a neural network trained by minimizing the PDE residual over sampled collocation points, and the gradient $\nabla_x v_n$ required for policy updates is obtained via automatic differentiation. This structure enables high-dimensional scalability and smooth feedback policy updates, at the expense of introducing approximation error.*

Since the practical algorithm employs neural network approximations and finite iterations, a theoretical justification of numerical errors is necessary. The next theorem quantifies how the total error can be controlled in terms of the residual at each step.

Theorem 2 (Global error of the practical PINN-PI algorithm). *Suppose Assumption 1 hold, and let $\{\tilde{v}_n, \tilde{\alpha}_n, \tilde{\beta}_n\}_{n \geq 0}$ be generated by Algorithm 2. If $\|\mathcal{R}_n\|_2 = p_n$ for*

$$\mathcal{R}_n := \partial_t \tilde{v}_n + L(t, x, \tilde{\alpha}_n \tilde{\beta}_n) + \frac{1}{2} \text{Tr}(\sigma \sigma^\top D^2 \tilde{v}_n),$$

there are constants $C > 0$ and $\rho \in (0, 1)$, depending only on $(d, \lambda, T, L_u, \kappa)$, such that

$$\sup_{t \in [0, T]} \|\tilde{v}_n(t, \cdot) - v(t, \cdot)\|_2 \leq C(p_n + \rho^n) \quad (3.10)$$

where (α_n, β_n) the exact feedback pair obtained from v_{n-1} .

Proof. Fix $n \geq 2$. Recall the decomposition

$$e_n := \tilde{v}_n - v = \underbrace{\tilde{v}_n - \hat{v}_n}_{:=A_n} + \underbrace{\hat{v}_n - v_n}_{:=B_n} + \underbrace{v_n - v}_{:=C_n},$$

where \hat{v}_n solves the linear PDE obtained by freezing the policies $(\tilde{\alpha}_n, \tilde{\beta}_n)$, and (α_n, β_n) is the exact policy pair obtained from v_{n-1} as in Theorem 1.

For simplicity as in Proposition 1, we reverse the time for all PDEs considered so that the terminal condition transforms to the initial condition, i.e., $v_n(0, x) = \hat{v}_n(0, x) = g(x)$ and $\tilde{v}_n(0, x)$ satisfies

$$\|\tilde{v}_n(0, x) - v_n(0, x)\| = 0.$$

Now subtracting the PDE for \hat{v}_n from the one for \tilde{v}_n , we derive that

$$\sup_{t \in [0, T]} \|A_n(t, \cdot)\|_2 \leq Cp_n$$

by Proposition 2.

For B_n , we note that

$$\begin{cases} \partial_t B_n + \frac{1}{2} \text{Tr}(\sigma \sigma^\top D^2 B_n) =: -\mathcal{L}_n, & \text{in } (0, T] \times \mathbb{R}^d, \\ B_n(0, \cdot) = 0, & \text{on } \mathbb{R}^d. \end{cases}$$

where

$$\mathcal{L}_n = L(t, x, \nabla_x \hat{v}_n)(\tilde{\alpha}_n, \tilde{\beta}_n) - L(t, x, \nabla_x v_n)(\alpha_n, \beta_n)$$

satisfies

$$\begin{aligned} |\mathcal{L}_n| &\leq L_u(|\alpha_n - \tilde{\alpha}_n| + |\beta_n - \tilde{\beta}_n|) \\ &\leq \kappa L_u |\nabla_x(\tilde{v}_{n-1} - v_{n-1})|, \quad \text{by Lemma 1} \end{aligned}$$

Applying the parabolic L^2 -estimate of Proposition 2 to the PDE satisfied by B_n and using the bound above, we obtain

$$\begin{aligned} \sup_{t \in [0, T]} \|B_n(t, \cdot)\|_2 &\leq C \|\mathcal{L}_n\|_2 \\ &\leq C \underbrace{\sup_{t \in [0, T]} \|(\nabla_x(\tilde{v}_{n-1}(t, \cdot) - v_{n-1}(t, \cdot)))\|_2}_{=: F_{n-1}} \end{aligned}$$

Invoking the same argument presented in Proposition 1, we have that $\tilde{\delta}_{n-1} := \tilde{v}_{n-1} - v_{n-1}$ satisfies

$$\|\nabla_x \tilde{\delta}_n(t, \cdot)\|_2 \leq \tilde{C} \sqrt{T} F_{n-2},$$

which leads to $F_n \leq \eta F_{n-2}$ for some $\eta \in (0, 1)$ for T sufficiently small.

For estimate of $C_n = v_n - v$, we recall Proposition 1, and obtain

$$\sup_{t \in [0, T]} \|C_n(t, \cdot)\|_2 \leq C \rho^n.$$

Combining the bounds for A_n , B_n , C_n , we have

$$\sup_{t \in [0, T]} \|\tilde{v}_n(t, \cdot) - v(t, \cdot)\|_2 \leq C(p_n + \eta^n + \rho^n) \leq C(p_n + \tilde{\rho}^n),$$

for some $\tilde{\rho} \in (0, 1)$. Repeating the argument on subintervals, $[0, T^*]$, $[T^*, 2T^*]$, ..., we finish the proof. \square

This result highlights a key advantage of the proposed framework: unlike black-box direct PINN solvers, the iterative structure permits explicit L^2 error estimates with provable rates. This is particularly important in nonconvex settings, where bounding the solution error is otherwise analytically intractable.

Furthermore, each iteration returns a practical, near-optimal feedback policy via simple pointwise mini-max updates, eliminating the need for any additional optimization.

4 Experimental results

To demonstrate the effectiveness of our policy iteration scheme for solving nonconvex viscous HJI equations, we consider a two-dimensional optimal path planning problem in the presence of a moving obstacle. The setting is cast as a two-player zero-sum differential game, where the robot aims to reach a target while minimizing cost, and the environment acts as an adversarial player introducing worst-case disturbances. To assess scalability, we also apply our method to a high-dimensional publisher-subscriber game, where multiple agents interact under stochastic dynamics with anisotropic noise. Although no ground truth is available in this setting, the learned value functions exhibit symmetric structures that align with the problem’s design.

4.1 Implementation Setup

This section details the implementation aspects of our work, including the neural network architecture, training configuration, policy iteration setup, and construction of reference solutions.

Neural Network Architecture As demonstrated in Section 3.2, we parameterize the value function $v_n(t, x; \theta_n) = g(x) + (T - t)\mathcal{N}_n(t, x; \theta_n)$, thereby the terminal condition is satisfied automatically. We model \mathcal{N}_n using a fully connected feedforward neural network (see Appendix C for details). In the neural network, we employ sinusoidal activation functions:

$$\phi_i(v) = \sin(W_i v + b_i),$$

as they are known to capture high-frequency structure and gradients more effectively than traditional activations [21]. In high-dimensional reachability tasks, sine-based networks have also been shown to reduce mean squared errors by an order of magnitude compared to ReLU or tanh activations [1].

Training Configuration We use the Adam optimizer [14] with a fixed learning rate of 0.001. All implementations are carried out using the JAX framework, which enables efficient automatic differentiation and GPU acceleration. All experiments were conducted on a workstation equipped with dual Intel Xeon Silver 4214R CPUs (2.4GHz) and an NVIDIA Quadro RTX 6000 GPU.

Policy Iteration Setup Our policy iteration scheme follows Algorithm 2. Problem-specific settings for the number of epochs E , policy updates M , and collocation points are detailed in Appendix C.

Reference Solution To quantitatively evaluate the accuracy of the learned value functions, we compute reference solutions to the HJI equation using an explicit finite difference method on a uniform grid. We employ backward time integration with central differences in space, and discretize the diffusion term using a second-order scheme, with homogeneous Neumann boundary conditions imposed on the spatial domain. To maintain stability in the presence of diffusion, the time and space steps are chosen such that $\Delta t = \Delta x^2$. The resulting numerical solutions approximate the viscosity solution and are used to compute the relative L^2 errors.

4.2 Two-dimensional optimal path planning with a moving obstacle

Let $X(s) \in \mathbb{R}^2$ denote the position of the robot at time $s \in [t, T]$. The system dynamics follow a controlled stochastic differential equation:

$$\begin{cases} dX(s) &= (a(s) + b(s))dt + \sigma dW_t, \quad \text{for } s \in (t, T], \\ X(t) &= x \in \mathbb{R}^2 \end{cases}$$

where $a(s)$ satisfying $|a(s)| \leq 1$ denotes the control input of the robot (Player I), $b(s)$ satisfying $|b(s)| \leq \delta$ for some $\delta > 0$ represents the adversarial disturbance (Player II), and $\sigma \in \mathbb{R}^{2 \times 2}$ is the noise matrix. Given $x_{\text{goal}} \in \mathbb{R}^2$ and weights λ_i for $i = 1, 2, 3$, the cost functional is defined as:

$$J(t, \mathbf{x}; a, b) = \mathbb{E} \left[\int_0^T (\lambda_1 |a(s)|^2 + \lambda_2 \phi(s, X(s))) ds + \lambda_3 |X(T) - x_{\text{goal}}|^2 \right],$$

where the obstacle penalty function $\phi(t, x)$ is given by:

$$\phi(s, x) = \exp\left(-\frac{\|x - x_{\text{obs}}(s)\|^2}{2\varepsilon^2}\right), \quad x_{\text{obs}}(s) = \begin{bmatrix} 0.5 \cos(\pi s) \\ 0.5 \sin(\pi s) \end{bmatrix}.$$

We define the value function

$$v(t, x) = \sup_{\beta \in \Gamma_t} \inf_{a \in \mathcal{A}_t} \mathbb{E} \left[\int_t^T c(s, x(s), a(s), \beta[a](s)) ds + g(x(T)) \right],$$

which is known to satisfy the viscous HJI equation

$$\begin{cases} \partial_t v + H(t, x, \nabla_x v) = -\frac{1}{2} \text{Tr}(\sigma \sigma^\top D_{xx}^2 v), & \text{in } (0, T) \times \mathbb{R}^d, \\ v(T, x) = g(x), & \text{on } \mathbb{R}^d. \end{cases}$$

with

$$H(t, x, p) = \sup_{\mathbf{b} \in B} \inf_{\mathbf{a} \in A} [\lambda_1 |\mathbf{a}|^2 + \lambda_2 \phi(t, x) + p(\mathbf{a} + \mathbf{b})].$$

for some $\lambda_1, \lambda_2 > 0$. Here, the Hamiltonian takes the closed form given by

$$H(t, x, p) = \begin{cases} -\frac{1}{4\lambda_1} |p|^2 + \lambda_2 \phi(t, x) + \delta |p|, & \text{if } |p| \leq 2\lambda_1, \\ -|p| + \lambda_1 + \lambda_2 \phi(t, x) + \delta |p|, & \text{otherwise.} \end{cases}$$

We solve the HJI equation using the PINN trained to minimize the residual of the PDE. Once the value function $v(t, x; \theta)$ is learned, the optimal control policy is recovered via:

$$a^*(t, x) = \begin{cases} -\frac{1}{2\lambda_1} \nabla_x v(t, x; \theta) & \text{if } \left| \frac{1}{2\lambda_1} \nabla_x v(t, x; \theta) \right| \leq 1, \\ -\frac{\nabla_x v(t, x; \theta)}{|\nabla_x v(t, x; \theta)|} & \text{otherwise.} \end{cases}$$

We set the simulation domain to $x \in [-1, 1]^2$ and the terminal time to $T = 1.0$. The optimization is configured with $\delta = 0.1$, $\lambda_1 = 0.1$, $\lambda_2 = 100$, $\lambda_3 = 10$, $\varepsilon = 0.3$, and the diffusion matrix is given by $\sigma = 0.1I_2$. The target position is fixed at $x_{\text{goal}} = (0.9, 0.9)$.

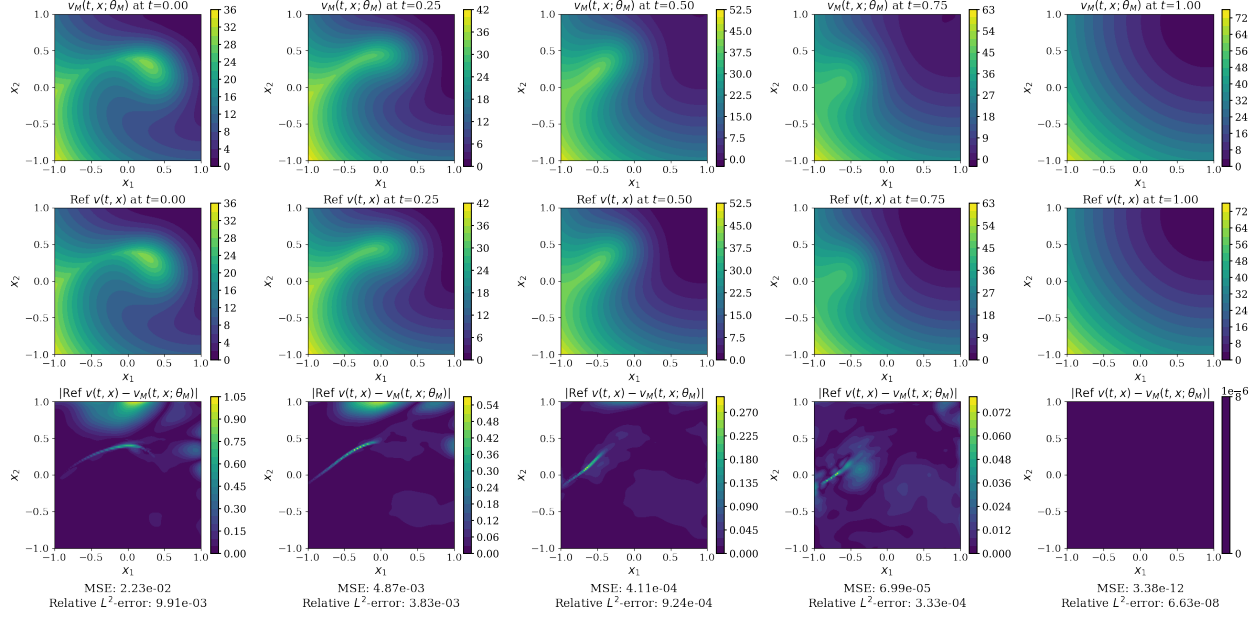


Figure 1: Comparison of the policy-iterative PINN solution and the reference FDM solution for the two-dimensional optimal path planning problem with a moving obstacle. Shown are the predicted value functions at selected times $t = 0.00, 0.25, 0.50, 0.75$, and 1.00 , along with absolute error plots and corresponding MSE and relative L^2 -error metrics.

Learning result In the 2D moving obstacle example, the finite difference solution is computed on an extended spatial domain to reduce boundary artifacts. The restricted solution over the target region is then used as a quantitative baseline for evaluating the learned value function.

Figure 1 compares the learned value function from the policy-iterative PINN with the reference solution obtained via finite differences, at five representative time points. The first two rows show the predicted and reference value functions, respectively, while the bottom row displays the pointwise absolute error, along with the corresponding MSE and relative L^2 -error. At all evaluated time instances, the policy-iterative PINN achieves consistently low errors, with relative L^2 -errors on the order of 10^{-3} or lower, demonstrating strong agreement with the reference solution.

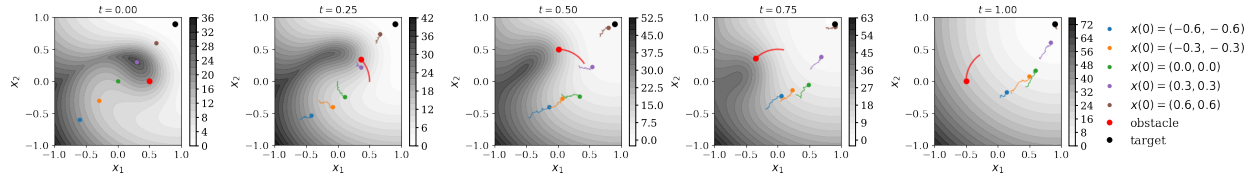


Figure 2: Time evolution of optimal trajectories derived from the policy-iterative PINN solution. Robots initialized at various positions navigate toward the target while avoiding a moving obstacle.

Figure 2 illustrates the time evolution of optimal trajectories computed from the learned value function obtained via the policy-iterative PINN. At each time step, control inputs are derived from the gradient of the learned value function, and the system dynamics are integrated using the Euler–Maruyama method [11]. The resulting trajectories show how the agents, starting from different initial positions, successfully avoid the moving obstacle and reach the target by the cost landscape encoded in the value function.

4.3 High-dimensional publisher-subscriber differential game

Let $x(t) \in \mathbb{R}^N$ denote the system state at time $t \in [0, T]$. It consists of a central publisher state $x_0(t)$ and $N-1$ subscriber states $x_1(t), \dots, x_{N-1}(t)$. A central agent (publisher) influences many followers (subscribers), each aiming to stay close to the leader while being disturbed. The system captures asymmetric interactions often seen in robotics, swarms, or communication networks. This system is governed by the following controlled stochastic differential equation:

$$dx(t) = f(x(t), u(t), d(t))dt + \sigma dW_t,$$

where $u(t) \in \mathcal{U} = \{\mathbf{u} \in \mathbb{R}^{N-1} : |\mathbf{u}| \leq 1\}$ is the control input (Player I), $d(t) \in \mathcal{D} = \{\mathbf{d} \in \mathbb{R}^{N-1} : |\mathbf{d}| \leq 1\}$ is the disturbance (Player II), and $\sigma \in \mathbb{R}^{N \times N}$ is the diffusion matrix. The drift term is compactly expressed as

$$f(x, u, d) = Ax + Bu + Cd + \psi(x),$$

where

$$A = e_1 e_1^\top - \mathbf{1}_N e_1^\top + a I_N, \quad B = \begin{bmatrix} 0 \\ b I_{N-1} \end{bmatrix}, \quad C = \begin{bmatrix} 0 \\ c I_{N-1} \end{bmatrix},$$

and the nonlinear interaction term is defined by

$$\psi(x) = \begin{bmatrix} \alpha \sin(x_0) \\ -\beta x_0 \end{bmatrix} \circ (x \circ x),$$

with \circ denoting the Hadamard (elementwise) product. The terminal cost is given by

$$g(x) = \frac{1}{2}((N-1)x_0^2 + \sum_{i=1}^{N-1} x_i^2 - (N-1)r^2),$$

which can equivalently be expressed as the sum of local costs over each publisher-subscriber pair:

$$g(x) = \sum_{i=1}^{N-1} g_i(P_i x), \quad g_i(P_i x) := \frac{1}{2}(x_0^2 + x_i^2 - r^2),$$

where $P_i : \mathbb{R}^N \rightarrow \mathbb{R}^2$ denotes the projection that extracts the (x_0, x_i) components, i.e., $P_i x = [x_0, x_i]^T$.

The combined structure of the separable cost and unidirectional dynamics leads to a value function that admits a decomposition of the form:

$$v(x, t) = \sum_{i=1}^{N-1} v_i(x_0, x_i, t),$$

where each v_i solves a two-dimensional HJI equation over the (x_0, x_i) subspace; see Appendix B for justification.

The corresponding Hamiltonian takes the form of

$$H(x, p) = p^\top (Ax + \psi(x)) - \|B^\top p\|_1 + \|C^\top p\|_1,$$

where $\|x\|_1 := \sum_{i=1}^N |x_i|$ for $x = (x_1, \dots, x_N)$. The HJI equation is solved using a PINN, and the optimal control and disturbance policies are recovered from the gradient of the learned value function as

$$u^*(x) = -\text{sign}(B^\top p), \quad \text{and} \quad d^*(x) = \text{sign}(C^\top p),$$

where the sign function is applied componentwise. We set the simulation domain to $x \in [-0.5, 0.5]^N$, terminal time $T = 0.5$, and parameter values $a = 1$, $b = 1$, $c = \frac{1}{2}$, $\alpha = -2$, and $\beta = 2$. The diffusion matrix is defined as $\sigma = 0.1I + P_\epsilon$, where P_ϵ is a symmetric matrix with zero diagonal and off-diagonal entries sampled from $\mathcal{U}(0, \epsilon)$. This formulation yields an isotropic setting when $\epsilon = 0$ and becomes anisotropic otherwise.

To solve the HJI equation, we consider both the proposed policy-iterative PINN and a direct PINN baseline. Both models share the same architecture, but differ in loss formulation and training schedule (see

Appendix C). The policy-iterative PINN minimizes the residual under fixed policies (see Section 4.1), while the direct PINN substitutes the closed-form Hamiltonian into the objective:

$$\mathcal{L}_{\text{Direct}}(\theta) = \frac{1}{N_{\text{int}}} \sum_{j=1}^{N_{\text{int}}} [\partial_t v(t_j, x_j; \theta) + H(x_j, \nabla_x v(t_j, x_j; \theta)) + \frac{1}{2} \text{Tr}(\sigma \sigma^\top D_{xx}^2 v(t_j, x_j; \theta))]^2.$$

Although the direct approach avoids explicit policy updates, the resulting loss involves non-smooth and nonlinear terms—such as l_1 norms of gradients, which may result in instability during training. The policy-iterative formulation mitigates this by decoupling the optimization into simpler fixed-policy subproblems. In all problem settings described below, we assess accuracy by comparing to a reference solution defined over an extended domain and restricted to the target region. Training is performed on the same domain to improve boundary behavior.

4.3.1 2D example - isotropic noise

We first consider the isotropic two-dimensional case ($\epsilon = 0$) to illustrate the method in a simple, visualizable setting.

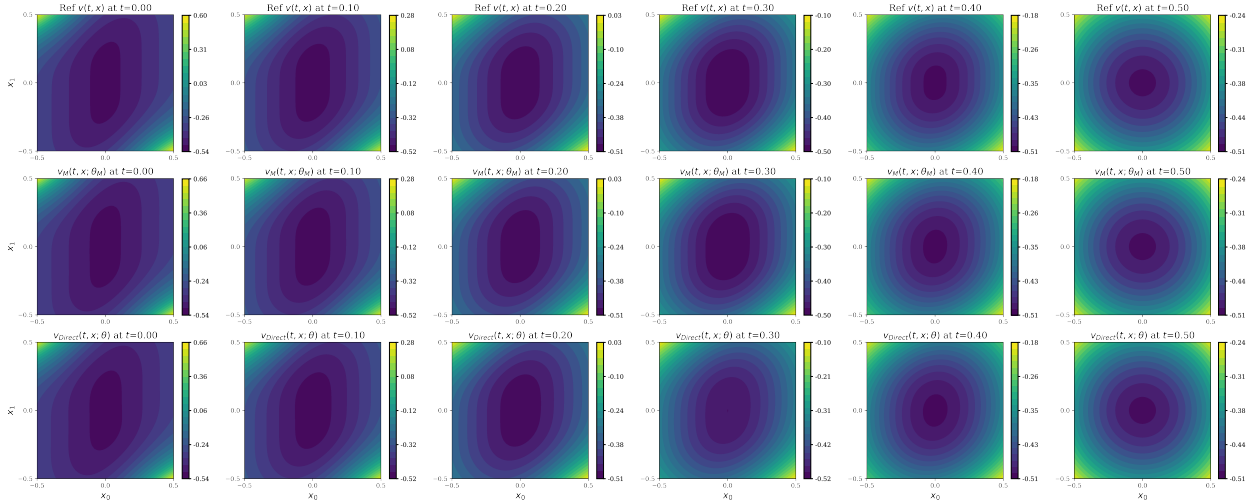


Figure 3: Comparison of policy-iterative and direct PINN approaches on the 2D isotropic benchmark problem. The first three rows show the learned value functions at selected times $t = 0.0, 0.1, \dots, 0.5$, with the top row corresponding to the reference solution, the second to the policy-iterative PINN, and the third to the direct PINN.

Table 1: Relative L^2 -errors and MSE over time for policy-iterative and direct PINN methods in the 2D isotropic setting. These results correspond to the time slices shown in Figure 3.

Method	Metric	$t = 0.0$	$t = 0.1$	$t = 0.2$	$t = 0.3$	$t = 0.4$	$t = 0.5$
PI	Rel. L^2	6.367e-03	1.272e-03	8.876e-04	6.484e-04	4.910e-04	3.705e-08
	MSE	6.007e-06	2.483e-07	1.263e-07	6.994e-08	4.122e-08	2.387e-16
Direct	Rel. L^2	7.241e-03	3.035e-03	2.429e-03	1.771e-03	1.055e-03	3.705e-08
	MSE	7.771e-06	1.430e-06	9.455e-07	5.218e-07	1.902e-07	2.387e-16

Learning result Figure 3 shows the learned value functions from the policy-iterative and direct PINN methods at selected times $t = 0.0, 0.1, \dots, 0.5$, alongside the reference solution. The corresponding MSE and relative L^2 -errors are summarized in Table 1 for each time step. At $t = 0$, both methods achieve relative

L^2 -errors on the order of 10^{-3} , indicating close agreement with the reference solution. Across all times, the policy-iterative PINN yields slightly improved accuracy in both error metrics.

4.3.2 5D example

We evaluate both PINN methods on a five-dimensional variant of the differential game under both isotropic ($\epsilon = 0$) and anisotropic ($\epsilon > 0$) noise settings. All configurations follow the high-dimensional setup described in Appendix C. To construct a reference solution, we exploit the separable structure of the isotropic case by summing four two-dimensional FDM solutions. We visualize the five-dimensional solution by projecting it onto the (x_0, x_i) subspace, setting all subscriber states same. This preserves the publisher-subscriber structure and enables 2D contour plots.

Learning result Figure 4 compares the learned value functions at $t = 0$ across increasing levels of anisotropy. The first column shows the reference solution in the isotropic case, while columns 2–5 show the results for increasing anisotropy. To ensure a fair comparison, the same random diffusion matrix σ is used for both methods at each $\epsilon > 0$. In the isotropic case, where decomposition is valid, the policy-iterative PINN achieves significantly lower errors across multiple time steps, as shown in Table 2, which reports both relative L^2 -errors and MSE from $t = 0$ to $t = 0.5$. For anisotropic settings, no ground-truth reference is available, so accuracy is assessed qualitatively. While the value function does not exhibit global symmetry, our 2D slice fixes x_0 and sets all subscriber states equal. In this configuration, the symmetric diffusion matrix induces identical noise across subscribers, so the solution is expected to appear symmetric about the $x_i = x_j$ axis. The policy-iterative PINN more closely preserves this structure and yields smoother level sets near the origin, indicating enhanced robustness under anisotropic diffusion.

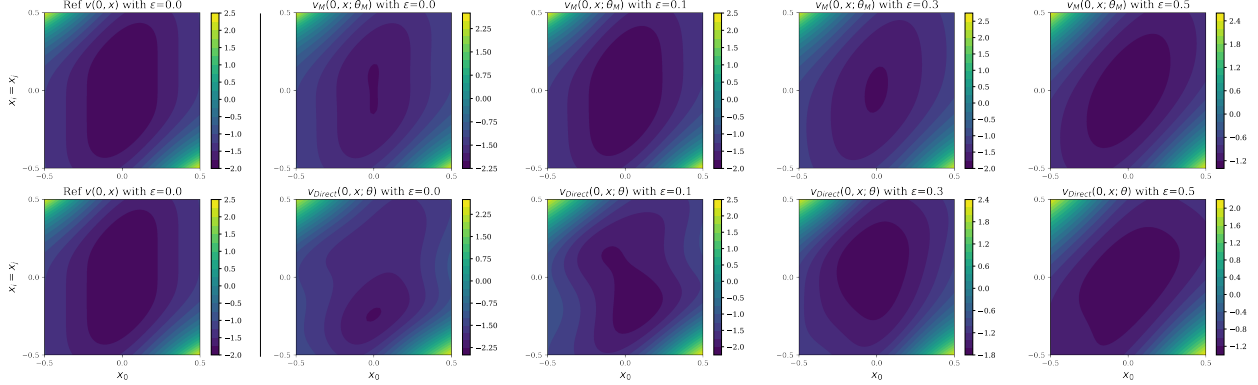


Figure 4: Comparison of policy-iterative and direct PINN methods on the five-dimensional anisotropic problem. The first column shows the summed reference solution over all (x_0, x_i) subspaces in the isotropic case ($\epsilon = 0$), while columns 2–5 display the learned value functions at $t = 0$ for varying levels of anisotropy ($\epsilon = 0.0, 0.1, 0.3, 0.5$)

Table 2: Relative L^2 -errors and MSE over time for policy-iterative and direct PINN methods in the 5D isotropic setting.

Method	Metric	$t = 0.0$	$t = 0.1$	$t = 0.2$	$t = 0.3$	$t = 0.4$	$t = 0.5$
PI	Rel. L^2	1.174e-02	8.283e-03	6.834e-03	5.028e-03	2.880e-03	3.705e-08
	MSE	3.269e-04	1.684e-04	1.198e-04	6.729e-05	2.268e-05	3.819e-15
Direct	Rel. L^2	1.120e-01	6.866e-02	4.697e-02	3.761e-02	2.214e-02	3.705e-08
	MSE	2.973e-02	1.157e-02	5.657e-03	3.765e-03	1.340e-03	3.819e-15

4.3.3 10D example

We extend the evaluation to the ten-dimensional setting, under both isotropic ($\epsilon = 0$) and anisotropic ($\epsilon > 0$) noise, using the same experimental configuration and visualization strategy as in the five-dimensional case.

Learning result Figure 5 shows the learned value functions at $t = 0$ for $\epsilon = 0.0, 0.1, 0.3$, and 0.5 , projected onto the (x_0, x_i) subspace. As in the five-dimensional case, the policy-iterative PINN produces smoother and more symmetric solutions across all noise levels. Table 3 reports the corresponding MSE and relative L^2 -errors from $t = 0$ to $t = 0.5$; even under isotropic noise, approximation errors are slightly higher than in the 5D setting due to the increased dimensionality.

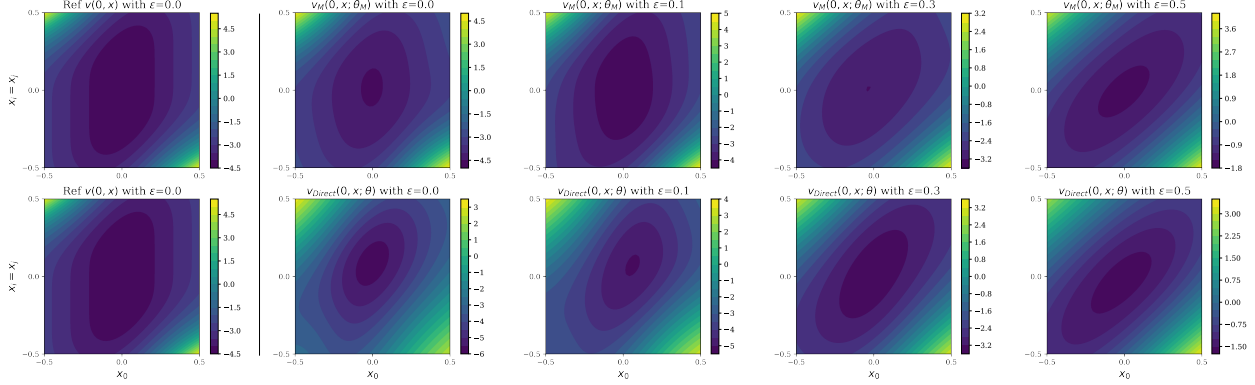


Figure 5: Comparison of policy-iterative and direct PINN methods on the ten-dimensional anisotropic problem. The first column shows the summed reference solution over all (x_0, x_i) subspaces in the isotropic case ($\epsilon = 0$), while columns 2–5 display the learned value functions at $t = 0$ for varying levels of anisotropy ($\epsilon = 0.0, 0.1, 0.3, 0.5$)

Table 3: Relative L^2 -errors and MSE over time for policy-iterative and direct PINN methods in the 10D isotropic setting.

Method	Metric	$t = 0.0$	$t = 0.1$	$t = 0.2$	$t = 0.3$	$t = 0.4$	$t = 0.5$
PI	Rel. L^2	5.804e-02	3.013e-02	1.308e-02	1.069e-02	8.953e-03	3.838e-08
	MSE	4.043e-02	1.128e-02	2.222e-03	1.539e-03	1.110e-03	2.074e-14
Direct	Rel. L^2	1.962e-01	1.355e-01	8.513e-02	4.739e-02	2.792e-02	3.838e-08
	MSE	4.623e-01	2.282e-01	9.409e-02	3.027e-02	1.079e-02	2.074e-14

5 Conclusion

In this work, we have proposed a novel mesh-free framework for solving nonconvex Hamilton–Jacobi–Isaacs (HJI) equations by combining classical policy iteration with physics-informed neural networks (PINNs). By leveraging the differentiability and expressive capacity of deep neural networks, the proposed method enables efficient approximation of viscosity solutions to high-dimensional HJI equations, even in the presence of nonconvexities in the Hamiltonian. We have provided a rigorous convergence analysis under a uniform ellipticity condition and demonstrated the numerical effectiveness of the method across several benchmark differential games in two to ten dimensions.

The experiments confirm that our approach not only achieves competitive accuracy but also enjoys scalability with respect to problem dimensionality, compared to standard PINN and direct collocation methods. Moreover, empirical results show that the iterative policy-improvement scheme yields lower residuals than

direct one-shot training and produces smoother, symmetry-consistent value functions even in highly non-convex settings. This is attributed to the fact that each policy-evaluation step solves a linearized PDE with fixed control inputs, resulting in smoother and more stable optimization dynamics. As a result, the learned value functions are not only more accurate but also exhibit desirable structural properties, such as symmetry and smoothness, even in highly nonconvex settings.

Furthermore, unlike direct one-shot approaches, our iterative framework enables systematic quantification of approximation errors. In particular, the L^2 error between the learned and true value functions can be rigorously bounded even in nonconvex settings, owing to the linearized structure of each policy evaluation step. Nevertheless, the method inherits limitations intrinsic to PINN-based approaches, such as sensitivity to network initialization and challenges in gradient stability over long training horizons.

An important limitation of the present work is the assumption of non-degenerate diffusion. In the absence of noise, the problem becomes a first-order Hamilton–Jacobi–Isaacs equation arising in deterministic differential games. This setting lacks the regularizing properties of second-order terms and poses distinct theoretical and computational challenges. We leave the development of PINN-based policy iteration schemes for such first-order HJI problems to future work.

Future work will aim to address these issues by incorporating adaptive sampling strategies, exploring PINN variants based on operator learning (e.g., DeepONet, FNO), and extending the framework to stochastic differential games and time-varying dynamics. The integration of our PINN-based policy iteration with model-based reinforcement learning paradigms also presents an exciting direction for further research.

Acknowledgement

Yeoneung Kim is supported by the National Research Foundation of Korea (NRF) grant funded by the Korea government(MSIT) (RS-2023-00219980, RS-2023-00211503). Hee Jun Yang and Minjung Gim are supported by National Institute for Mathematical Sciences(NIMS) grant funded by the Korea government(MSIT) (No. B25810000). The authors would like to thank Professor Hung Vinh Tran (University of Wisconsin–Madison) for his insightful suggestions and valuable guidance in developing and refining the ideas of this work.

References

- [1] S. Bansal and C. J. Tomlin. Deepreach: A deep learning approach to high-dimensional reachability. In *Proc. IEEE Int. Conf. Robot. Autom.*, pages 1817–1824. IEEE, 2021.
- [2] G. Barles and P. E. Souganidis. Convergence of approximation schemes for fully nonlinear second order equations. *Asymptot. Anal.*, 4(3):271–283, 1991.
- [3] T. J. Barth and J. A. Sethian. Numerical schemes for the hamilton–jacobi and level set equations on triangulated domains. *J. Comput. Phys.*, 145(1):1–40, 1998.
- [4] T. Cecil, J. Qian, and Stanley Osher. Numerical methods for high dimensional Hamilton–Jacobi equations using radial basis functions. *J. Comput. Phys.*, 196(1):327–347, 2004.
- [5] M. G. Crandall, H. Ishii, and P.L. Lions. User’s Guide to viscosity solutions of second order partial differential equations. *Bull. Amer. Math. Soc.*, 27(1):1–67, 1992.
- [6] L. C. Evans. *Partial Differential Equations*, volume 19 of *Grad. Stud. Math.* Amer. Math. Soc., 2022.
- [7] R. Ferretti and O. Junge. An adaptive multilevel radial basis function scheme for the hjb equation. In *Proceedings of the SSSC Workshop (SpecSem 2016)*, 2016.
- [8] W. H. Fleming and H. M. Soner. *Controlled Markov processes and viscosity solutions*, volume 25. Springer Science & Business Media, 2006.
- [9] X. Guo, H. V. Tran, and Y. P. Zhang. Policy iteration for nonconvex viscous Hamilton–Jacobi equations. *arXiv preprint arXiv:2503.02159*, 2025.

- [10] J. Han, A. Jentzen, and W. E. Solving high-dimensional partial differential equations using deep learning. *Proc. Natl. Acad. Sci.*, 115(34):8505–8510, 2018.
- [11] D. J. Higham. An algorithmic introduction to numerical simulation of stochastic differential equations. *SIAM Review*, 43(3):525–546, 2001.
- [12] E. L. Kawecki and T. Sprekeler. Discontinuous galerkin and c0-ip finite element approximation of periodic hamilton–jacobi–bellman–isaacs problems with application to numerical homogenization. *ESAIM: Math. Model. Numer. Anal.*, 56(2):679–704, 2022.
- [13] B. Kerimkulov, D. Siska, and L. Szpruch. Exponential convergence and stability of howard’s policy improvement algorithm for controlled diffusions. *SIAM J. Control Optim.*, 58(3):1314–1340, 2020.
- [14] D. P. Kingma and J. Ba. Adam: A method for stochastic optimization. *arXiv preprint arXiv:1412.6980*, 2014.
- [15] M. V. Klibanov, L. H. Nguyen, and H. V. Tran. Numerical viscosity solutions to hamilton–jacobi equations via a carleman estimate and the convexification method. *J. Comput. Phys.*, 451:110828, 2022.
- [16] H. J. Kushner. Numerical methods for stochastic control problems in continuous time. *SIAM J. Control Optim.*, 28(5):999–1048, 1990.
- [17] I. E. Lagaris, A. Likas, and Dimitrios I. Fotiadis. Artificial neural networks for solving ordinary and partial differential equations. *IEEE Trans. Neural Netw. Learn. Syst.*, 9(5):987–1000, 1998.
- [18] J. Y. Lee and Y. Kim. Hamilton–jacobi based policy-iteration via deep operator learning. *Neurocomputing*, page 130515, 2025.
- [19] Y. Liu, L. Cai, Y. Chen, and B. Wang. Physics-informed neural networks based on adaptive weighted loss functions for hamilton-jacobi equations. *Math. Biosci. Eng.*, 19(12):12866–12896, 2022.
- [20] M. Raissi, P. Perdikaris, and G. E. Karniadakis. Physics-informed neural networks: A deep learning framework for solving forward and inverse problems involving nonlinear partial differential equations. *J. Comput. Phys.*, 378:686–707, 2019.
- [21] Vincent Sitzmann, Julien Martel, Alexander Bergman, David Lindell, and Gordon Wetzstein. Implicit neural representations with periodic activation functions. *Adv. Neural. Inf. Process. Syst.*, 33:7462–7473, 2020.
- [22] P. E. Souganidis. Approximation schemes for viscosity solutions of hamilton-jacobi equations. *Differential Equations*, 59(1):1–43, 1985.
- [23] W. Tang, H. V. Tran, and Y. P. Zhang. Policy iteration for the deterministic control problems—a viscosity approach. *SIAM J. Control Optim.*, 63(1):375–401, 2025.
- [24] H. V. Tran, Z. Wang, and Y. P. Zhang. Policy iteration for exploratory hamilton–jacobi–bellman equations. *Appl. Math. Optim.*, 91(2):50, 2025.
- [25] M. Zhou and J. Lu. Solving time-continuous stochastic optimal control problems: Algorithm design and convergence analysis of actor-critic flow. *arXiv preprint arXiv:2402.17208*, 2024.

A Parabolic L^2 estimate

Proposition 2 (Parabolic L^2 -estimate). *Let $d \in \mathbb{N}$ and $T > 0$. Suppose Assumption 1 holds. Let $b \in L^\infty((0, T) \times \mathbb{R}^d)$, $P \in L^2((0, T); L^2(\mathbb{R}^d))$ and $Q \in L^2(\mathbb{R}^d)$. For $n \geq 1$ fixed, let v be a unique viscosity solution of*

$$\begin{cases} \partial_t v + \frac{1}{2} \text{Tr}(\sigma \sigma^\top D_{xx}^2 v) + b(t, x) \cdot \nabla_x v = P(t, x), & \text{in } [0, T) \times \mathbb{R}^d, \\ v(T, x) = Q(x) & \text{on } \mathbb{R}^d. \end{cases} \quad (\text{A.1})$$

Then we have

$$\frac{d}{dt} \|v(t, \cdot)\|_2^2 + \lambda \|\nabla_x v(t, \cdot)\|_2^2 \leq \left(\frac{2\|b\|_\infty^2}{\lambda} + 1\right) \|v(t, \cdot)\|_2^2 + \|P(t, \cdot)\|_2^2.$$

Therefore, there exists a constant $C_T = C(d, \lambda, T, \|b\|_\infty) > 0$, independent of n , such that

$$\sup_{t \in [0, T]} \|v(t, \cdot)\|_2^2 + \lambda \int_0^T \|\nabla_x v(t, \cdot)\|_2^2 dt \leq C_T (\|Q\|_2^2 + \|P\|_2^2).$$

B Proof of Value Function Decomposition

We show that the value function $v(x, t)$ associated with the high-dimensional HJI equation admits an exact decomposition across publisher-subscriber pairs, provided that the terminal cost is separable and the dynamics are unidirectionally coupled.

Let $x = [x_0, x_1, \dots, x_{N-1}]^\top \in \mathbb{R}^N$ be the full state vector, where x_0 is the publisher state and x_i is the i -th subscriber state. The terminal cost is given by a sum of pairwise costs:

$$g(x) = \sum_{i=1}^{N-1} g_i(P_i x), \quad g_i(P_i x) = \frac{1}{2}(x_0^2 + x_i^2 - r^2),$$

where $P_i : \mathbb{R}^N \rightarrow \mathbb{R}^2$ denotes the projection $P_i x = [x_0, x_i]^\top$.

Let v denote the viscosity solution of the full HJI equation:

$$\begin{cases} \partial_t v + H(t, x, \nabla v) = -\frac{1}{2} \text{Tr}(\sigma \sigma^\top D^2 v), & \text{in } (0, T) \times \mathbb{R}^d, \\ v(T, x) = g(x), & \text{on } \mathbb{R}^d. \end{cases}$$

We define the candidate decomposed value function as

$$\hat{v}(x, t) := \sum_{i=1}^{N-1} v_i(x_0, x_i, t),$$

where each v_i solves a two-dimensional HJI equation on the projected subspace (x_0, x_i) :

$$\begin{cases} \partial_t v_i + H_i(t, x_0, x_i, \partial_{x_0} v_i, \partial_{x_i} v_i) = -\frac{1}{2} \text{Tr}(\sigma_i \sigma_i^\top D_{xx}^2 v_i), & \text{in } (0, T) \times \mathbb{R}^2, \\ v_i(T, x_0, x_i) = g_i(x_0, x_i) & \text{on } \mathbb{R}^2. \end{cases}$$

Here, H_i denotes the reduced Hamiltonian obtained by restricting the dynamics and control inputs to the (x_0, x_i) subspace, consistent with the unidirectional structure of the system.

We assume each v_i is a viscosity solution with sufficient regularity for the chain rule and distributional derivatives to apply. The second-order term $\sigma \sigma^\top$ is assumed to decompose across each (x_0, x_i) subspace, which is the case when σ is block-diagonal or isotropic. Each σ_i is the submatrix of σ corresponding to the (x_0, x_i) coordinates. Under this assumption,

$$\text{Tr}(\sigma \sigma^\top D_{xx}^2 \hat{v}) = \sum_{i=1}^{N-1} \text{Tr}(\sigma_i \sigma_i^\top D_{xx}^2 v_i).$$

Since each v_i depends only on (x_0, x_i) , the full time and spatial derivatives of \hat{v} decompose as:

$$\partial_t \hat{v} = \sum_{i=1}^{N-1} \partial_t v_i, \quad \text{and} \quad \nabla_x \hat{v} = \sum_{i=1}^{N-1} \nabla_{x_0, x_i} v_i,$$

where $\nabla_{x_0, x_i} v_i$ is understood to be embedded in \mathbb{R}^N with zeros in all other coordinates. (e.g., the gradient is zero in all coordinates except the x_0 and x_i entries). Since the dynamics are unidirectional, each H_i depends only on (x_0, x_i) , allowing the full Hamiltonian to be written as a sum of local terms.

$$H(t, x, \nabla \hat{v}) = \sum_{i=1}^{N-1} H_i(t, x_0, x_i, \nabla_{x_0, x_i} v_i),$$

where $\nabla_{x_0, x_i} v_i$ denotes the pair $(\partial_{x_0} v_i, \partial_{x_i} v_i)$. It follows that \hat{v} satisfies the same PDE as v , almost everywhere.

By the construction of \hat{v} and the separability of g ,

$$\hat{v}(x, T) = \sum_{i=1}^{N-1} v_i(x_0, x_i, T) = \sum_{i=1}^{N-1} g_i(x_0, x_i) = g(x).$$

Since the HJI equation admits a unique viscosity solution under Lipschitz and uniformly elliptic conditions, it follows that $v(x, t) = \hat{v}(x, t)$, and the decomposition holds globally.

C Details of Implementation Parameters

Table 4: Summary of numerical settings for each experiment

Setting	Moving Obstacle (2D)	Publisher–Subscriber (ND)
Neural Network Settings		
Network architecture	4 hidden layers, 64 units	3 hidden layers, 64 units
Training epochs per iteration (E)	1,000	5,000
Policy iteration (M)	1,000	500
Direct PINN epoch ($E \times M$)		2,500,000
Collocation points	2,000 (refreshed every 100 epochs)	$N \times 1,000$ (refreshed every 100 epochs)
Initial policy	Uniform over admissible set	Uniform over admissible set
Extended spatial domain	$[-1, 1]^2$	$[-1.5, 1.5]^N$
Target domain	$[-1, 1]^2$	$[-0.5, 0.5]^N$
Reference Solution Settings		
Extended spatial domain	$[-2, 2]^2$	$[-1.5, 1.5]^N$
Target domain	$[-1, 1]^2$	$[-0.5, 0.5]^N$
FDM spatial grid	201×201	151×151
FDM time steps	201^2	151^2
Boundary condition	Homogeneous Neumann	Homogeneous Neumann